THE ASTROPHYSICAL JOURNAL SUPPLEMENT SERIES, 126:537–550, 2000 February

ELECTRON-ION RECOMBINATION RATE COEFFICIENTS AND PHOTOIONIZATION CROSS SECTIONS FOR ASTROPHYSICALLY ABUNDANT ELEMENTS. III. Si-SEQUENCE IONS: Si I, S III, Ar V, Ca VII, AND Fe XIII

SULTANA N. NAHAR
Department of Astronomy, Ohio State University, Columbus, OH 43210
Received 1999 July 1; accepted 1999 September 16

ABSTRACT

Photoionization cross sections, σ_{PI}, and electron-ion recombination rate coefficients, α_R, for silicon-like ions are calculated. Calculations are carried out in the close coupling approximation using the ***R***-matrix method. Each ion has a large number of bound states with $n \leq 10$ and $l \leq 9$: 433 for Ar V, 631 for Ca VII, and 1223 for Fe XIII. Both the partial photoionization cross sections leaving the core ion in the ground state and the total cross sections for ionization in the ground state as well as the excited core states are obtained for all bound states. The electron-ion recombination rates are obtained using a unified method, based on the close coupling ***R***-matrix method, that incorporates both the radiative and dielectronic recombination processes in a self-consistent and unified manner. Total recombination rate coefficients are presented for a wide range of temperatures for practical applications. State-specific recombination rate coefficients for individual bound states are also presented. Results of Si I and S III, derived from earlier works, are also presented for completeness.

Subject headings: atomic data — atomic processes

1. INTRODUCTION

The aim of the present work is to provide accurate and self-consistent results for photoionization cross sections, σ_{PI}, and total and state-specific electron-ion recombination rate coefficients of atoms and ions for various astrophysical applications. Electron-ion recombination is an important process in plasmas in both photoionization equilibrium and coronal equilibrium. Self-consistent atomic parameters are needed for the inverse processes of photoionization and recombination in order to avoid uncertainties introduced by different approximations, heretofore employed in ionization balance calculations. Present work satisfies the consistency criterion by calculating σ_{PI} and α_R in the close coupling approximation using the same set of atomic wave functions.

Furthermore, the recently introduced unified treatment of total (electron + ion) recombination (Nahar & Pradhan 1994, 1995) enables the consideration of radiative and dielectronic recombination processes (RR and DR, respectively) in a unified and ab initio manner. Most of the electron-ion recombination data employed in earlier works is based on RR rates (e.g., Aldrovandi & Pequignot 1974) derived from photoionization cross sections that neglect the now well-established phenomenon of autoionizing resonances. The DR rates at high temperature are usually derived from the Burgess general formula (Burgess 1965) or by incorporating the treatment of the DR by Jacobs et al. (1977), who showed the effect of autoionization into excited states, and at low temperatures by Nussbaumer & Storey (1983), who included the contribution from near-threshold autoionizing resonances resulting in a low-temperature enhancement in the DR rate. The total recombination rate coefficients are then obtained from the sum of the RR and from the low- and high-temperature DR rate coefficients.

In the first two papers of the series, photoionization cross sections, recombination rate coefficients, and ionization fractions were presented for isonuclear sequences: all ions of carbon and nitrogen (Nahar & Pradhan 1997) and oxygen (Nahar 1999a). The present work reports photoionization cross sections and recombination rate coefficients of ions along an isoelectronic sequence: the Si-like ions.

This report presents results for silicon-like ions, Ar V, Ca VII, and Fe XIII. Sample results of Si I and S III from earlier calculations (Nahar 1995, 1996a) are also presented for completeness. Calculations for isoelectronic sequences are often facilitated by the use of the same algebraic formulations for the target expansion of all ions in the sequence. However, this is not the case for Si-sequence ions for which each target ion has a different expansion since the *LS* terms are not in the same order for all ions. The radiative data for a large number of oscillator strengths and photoionization cross sections for these ions were obtained under the Opacity Project (OP; Seaton 1987; The Opacity Project Team 1995–1996). The calculations for Si I, S III, Ar V, and Ca VII were carried out by Nahar & Pradhan (1993) and for Fe XIII by K. Butler, C. Mendoza, & C. J. Zeippen (2000, in preparation). The work by Butler et al. has not been published yet; however, the results are available through the OP electronic database TOPbase (Cunto et al. 1993). Present calculations are carried out using larger eigenfunction expansions, with more target states, and the computations are therefore more extensive than the previous ones. A much larger amount of data is obtained in the present work. Also, the cross sections obtained under the OP are *total*; i.e., the ionization corresponds to leaving the core in the ground as well as in the excited states. However, for calculations of electron-ion recombination, the *partial* cross sections leaving the core in the ground state are required. Hence, it is necessary to carry out the calculations in their entirety.

2. THEORY AND COMPUTATIONS

The calculations are carried out in the close coupling (CC) approximation using the ***R***-matrix method (Seaton 1987). In the CC approximation, the target or the core ion is represented by an N-electron system, and the $(N + 1)$th electron is bound or in the continuum. The total wave func-

tion, $\Psi(E)$, of the $(N + 1)$-electron system for any symmetry $SL\pi$ is represented by an expansion of the eigenfunctions of the core or the target ion, coupled to the $(N + 1)$th electron, as

$$\Psi_E(\text{ion} + e) = A \sum_i \chi_i(\text{ion})\theta_i + \sum_j c_j \Phi_j , \qquad (1)$$

where χ_i is the target wave function in a specific state $S_i L_i \pi_i$, and θ_i is the wave function for the $(N + 1)$th electron in a channel labeled $S_i L_i \pi_i k_i^2 \ell_i(SL\pi)$, k_i^2 being its kinetic energy. The Φ_j's are bound channel functions of the $(N + 1)$-electron system that account for the short-range correlation and the orthogonality between the continuum and the bound electron orbitals. Electron-ion states with $E \leq 0$ are bound states, Ψ_B, and those with $E > 0$ are continuum states, Ψ_F. The complex resonant structures in photoionization and recombination result from channel couplings between continuum channels that are open ($k_i^2 > 0$) and ones that are closed ($k_i^2 < 0$) at electron energies k_i^2 corresponding to the Rydberg series converging to the target thresholds.

In the present work, each ion is represented by a larger wave function expansion (presented in Table 1) than used in previous calculations (Nahar & Pradhan 1993; K. Butler et al. 2000, in preparation). The expansion consists of 17 terms of Ar VI (compared with 13 in the earlier works), 19 terms of Ca VIII (compared with 18), and 14 terms of Fe XIV (compared with 9). In Table 1, the target energies that are not experimentally observed are marked with asterisks. Target terms in the CC eigenfunction expansion for Si II and S IV are also given in Table 1. For accurate positions of resonances in the photoionization cross sections, the calculated target energies are replaced by the observed ones. Since not all the target terms have been observed, calculated energies are used for the terms not observed. Of the two closely lying Fe XIV states, $3s3p3d(^4D^o)$ and $3s3p3d(^2D^o)$, only the former has been observed. To maintain the right energy order, the $^2D^o$ lying above the $^4D^o$ as obtained from atomic structure calculations, calculated energies are used for both the terms. The energies and the target wave functions are obtained from atomic structure calculations using the code SUPERSTRUCTURE (Eissner, Jones, & Nussbaumer 1974). The list of spectroscopic and correlation configurations and the values of the scaling parameter, λ_{nl}, for each orbital in the Thomas-Fermi-Dirac potential used in the atomic structure calculations are provided in Table 1.

The second sum in the wave function expansion, equation (1), includes all possible $(N + 1)$-electron configurations of Ar V and Ca VII up to $3p^4$, $3d^2$, $4s^2$, and $4p$ and of

TABLE 1

TARGET TERMS IN THE EIGENFUNCTION EXPANSIONS OF Si-LIKE IONS

Si II: 8-CC		S IV: 16-CC		Ar VI: 17-CC		Ca VIII: 19-CC		Fe XIV: 14-CC	
Term	E(Ry)	Term	E(Ry)	Term	E(Ry)	Term	E(Ry)	Term	E(Ry)
$3s^23p(^2P^o)$...	0.0	$3s^23p(^2P^o)$	0.0	$3s^23p(^2P^o)$	0.0	$3s^23p(^2P^o)$	0.0	$3s^23p(^2P^o)$	0.0
$3s3p^2(^4P^e)$...	0.391865	$3s3p^2(^4P^e)$	0.653779	$3s3p^2(^4P^e)$	0.92440	$3s3p^2(^4P^e)$	1.19920	$3s3p^2(^4P^e)$	2.124574
$3s3p^2(^2D^e)$...	0.504103	$3s3p^2(^2D^e)$	0.857789	$3s3p^2(^2D^e)$	1.20772	$3s3p^2(^2D^e)$	1.56489	$3s3p^2(^2D^e)$	2.739109
$3s^24s(^2S^e)$ ...	0.596884	$3s3p^2(^2S^e)$	1.12550	$3s3p^2(^2S^e)$	1.54734	$3s3p^2(^2S^e)$	1.97367	$3s3p^2(^2S^e)$	3.323328
$3s3p^2(^2S^e)$ ...	0.698626	$3s3p^2(^2P^e)$	1.22143	$3s3p^2(^2P^e)$	1.66864	$3s3p^2(^2P^e)$	2.12083	$3s3p^2(^2P^e)$	3.588995
$3s^23d(^2D^e)$...	0.723076	$3s^23d(^2D^e)$	1.38641	$3s^23d(^2D^e)$	1.99231	$3s^23d(^2D^e)$	2.57423	$3s^23d(^2D^e)$	4.323243
$3s^24p(^2P^o)$...	0.740234	$3s^24s(^2S^e)$.....	1.68686	$3p^3(^2D^o)$	2.31660*	$3p^3(^2D^o)$	2.97221*	$3p^3(^2D^o)$	4.916485*
$3s3p^2(^2P^e)$...	0.764889	$3p^3(^2D^o)$	1.68686	$3p^3(^4S^o)$	2.46510	$3p^3(^4S^o)$	3.14637	$3p^3(^4S^o)$	5.341210
		$3p^3(^4S^o)$	1.79023	$3s3p3d(^4F^o)$...	2.62267*	$3s3p3d(^4F^o)$...	3.40421*	$3p^3(^2P^o)$.....	5.585664*
		$3s3p3d(^4F^o)$...	1.85816	$3p^3(^2P^o)$.....	2.69737*	$3p^3(^2P^o)$.....	3.41689*	$3s3p3d(^4F^o)$...	5.630238*
		$3p^3(^2P^o)$.....	1.94697	$3s3p3d(^4P^o)$...	2.88639	$3s3p3d(^4P^o)$...	3.72392	$3s3p3d(^4P^o)$...	6.074676*
		$3s^24p(^2P^o)$	1.94697	$3s3p3d(^4D^o)$...	2.91360	$3s3p3d(^4D^o)$...	3.76028	$3s3p3d(^4D^o)$...	6.116031
		$3s3p3d(^4P^o)$...	2.04607	$3s3p3d(^2D^o)$...	3.06291*	$3s3p3d(^2D^o)$...	3.91031*	$3s3p3d(^2D^o)$...	6.359663*
		$3s3p3d(^4D^o)$...	2.04607	$3s^24s(^2S^e)$.....	3.11914	$3s3p3d(^2F^o)$...	4.10628*	$3s3p3d(^2F^o)$...	6.677360*
		$3s3p3d(^2D^o)$...	2.20608	$3s3p3d(^2F^o)$...	3.20219*	$3s3p3d(^2P^o)$...	4.46793*		
		$3s3p3d(^2F^o)$...	2.20608	$3s3p3d(^2P^o)$...	3.51259*	$3s3p3d(^2F^o)$...	4.57831*		
				$3s3p3d(^2F^o)$...	3.59756*	$3s3p3d(^2D^o)$...	4.78299*		
						$3s3p3d(^2P^o)$...	4.79309*		
						$3s^24s(^2S^e)$.....	4.98757		

NOTE.—Unobserved terms are marked by asterisks. The set of spectroscopic and correlation configurations and the Thomas-Fermi scaling parameters λ_{nl} used in the atomic structure calculations are also given.

Si II.—Spectroscopic: $3s^23p$, $3s3p^2$, $3s^23d$, $3s^24s$, and $3s^24p$.

Correlation: $3p^3$, $3s3p3d$, $3s3p4s$, $3s3p4p$, $3s3p4d$, $3s3d4f$, $3s3d4s$, $3s3d4p$, $3s3d4d$, $3s^24d$, $3p3d4s$, $3p3d4p$, $3p3d4d$, $3p3d4f$, $3p^24s$, $3p^24p$, $3p^24d$, $3p^23d$, $3p3d^2$, and $3d^3$.

λ_{nl}: 1.0874(1s), 1.0874(2s), 1.0154(2p), 1.0449(3s), 1.03591(3p), 1.18176(3d), 1.1114(4s), 1.1515(4p), 1.50001(4d), and 2.99166(4f).

S IV.—Spectroscopic: $3s^23p$, $3s3p^2$, $3p^3$, $3s^23d$, $3s^24s$, $3s^24p$, and $3s3p3d$.

Correlation: $3s^24d$, $3s3p4s$, $3s3p4p$, $3s3p4d$, $3s3p4d$, $3s3d4s$, $3s3d4p$, $3s3d4d$, $3p^23d$, $3p^24s$, $3p^24p$, $3p^24d$, $3p3d4s$, $3p3d4p$, and $3p3d4d$.

λ_{nl}: 1.1(1s), 1.08576(2s), 1.03329(2p), 1.07439(3s), 1.04779(3p), 1.03206(3d), 1.14812(4s), 1.15514(4p), and 1.42067(4d).

Ar VI.—Spectroscopic: $3s^23p$, $3s3p^2$, $3p^3$, $3s^23d$, $3s3p3d$, and $3s^24s$.

Correlation: $3s^24p$, $3s3p4s$, $3s3p4p$, $3s3d4s$, $3s3d4p$, $3p^23d$, $3p^24s$, $3p^24p$, $3p3d4s$, and $3p3d4p$.

λ_{nl}: 1.1(1s), 1.08576(2s), 1.03329(2p), 1.05817(3s), 0.95008(3p), 1.11118(3d), 1.04572(4s), and 2.12666(4p).

Ca VIII.—Spectroscopic: $3s^23p$, $3s3p^2$, $3p^3$, $3s^23d$, $3s3p3d$, and $3s^24s$.

Correlation: $3s^24p$, $3s3p4s$, $3s3p4p$, $3s3d4s$, $3s3d4p$, $3p^23d$, $3p^24s$, $3p^24p$, $3p3d4s$, and $3p3d4p$.

λ_{nl}: 1.1(1s), 1.09(2s), 1.0(2p), 1.11(3s), 1.05(3p), 1.03(3d), 1.25(4s), and 3.0(4p).

Fe XIV.—Spectroscopic: $3s^23p$, $3s3p^2$, $3p^3$, $3s3p3d$, and $3p^23d$.

Correlation: $3s^24s$, $3s^24p$, $3s3p4s$, $3s3p4p$, $3s3d4s$, $3s3d4p$, $3p^24s$, $3p^24p$, $3p3d4s$, and $3p3d4p$.

λ_{nl}: 1.1(1s), 1.08576(2s), 1.03329(2p), 0.947(3s), 0.90957(3p), 1.00689(3d), 4.85982(4s), and 2.19876(4p).

Fe XIII up to $3p^4$, $3d^2$, $4s$, and $4p$. Computations include all $SL\pi$ symmetries of the ion formed from target states coupled with the outer electron with $l \leq 9$. The computations are carried out using the ***R***-matrix codes developed for the OP (Berrington et al. 1987), for the Iron Project (Hummer et al. 1993) and new extensions related to photoionization and recombination calculations as presented herein (Nahar & Pradhan 1994; Nahar 1996b).

2.1. *Bound States*

The (electron + ion) Hamiltonian matrix is scanned for the bound states up to $n = 10$ and $l = 9$ with an effective quantum number interval of $\Delta\nu = 0.01$. The three ions, Ar V, Ca VII, and Fe XIII, have a large number of bound states. Identification of these calculated LS bound states has been a major task for the ions, especially for Fe XIII (Nahar 1999b). Identification is carried out using quantum defect analysis and through channel contributions. The valence electron terms are formed with the core in one of the states considered in the wave function expansion (Table 1), while the equivalent electron states are formed by the addition of an electron to the outer orbital of the core (parent) configurations. However, small differences in effective quantum number ν for various terms of the same symmetry can cause difficulties in the proper assignment of the configurations. In addition, bound states corresponding to bound channel configurations (the second sum of eq. [1]) are also obtained, and these are not always well represented. These terms are assigned with possible configurations with the core of the forms $3s3d^2$, $3p3d^2$, and $3d^24s$. (The complete set of term energies for each ion will be available in the electronic file for state-specific recombination rate coefficients.) The total number of bound states, N_b^T, obtained with $n \leq 10$ and $l \leq 9$ is 433 for Ar V, 631 for Ca VII, and 1223 for Fe XIII. The total number of bound states for Si I is 265 and for S III is 309, obtained from earlier calculations. State-specific rates are obtained for all states, N_b, that couple to the target ground state. Table 3 lists all states, N_b^T and N_b.

2.2. *Total and Partial Photoionization Cross Sections*

The photoionization cross section may be expressed as

$$\sigma_{\rm PI} = \frac{1}{g}\frac{4\pi^2}{3c}\,\omega \boldsymbol{S}\,, \tag{2}$$

where g is the statistical weight factor of the bound state, $\boldsymbol{S}$ is the dipole line strength,

$$\boldsymbol{S} = |<\Psi_B||\boldsymbol{D}||\Psi_F>|^2\,, \tag{3}$$

and $\boldsymbol{D}$ is the dipole operator (e.g., Seaton 1987).

The Rydberg series of autoionizing resonances in $\sigma_{\rm PI}$ are resolved in detail. The resonance structures are resolved with $\Delta\nu = 0.01$ up to an effective quantum number, $\nu = 10$, i.e., at 100 energies for each interval $(\nu, \nu + 1)$. Furthermore, the near-threshold resonances that contribute predominantly to low-temperature recombination are resolved on a much finer energy mesh, with typically 2000 energies just above the ionization threshold. The resonance profiles decrease in width with effective quantum number as ν^{-3}, relative to the threshold of convergence such that $\nu(E) = z/(E - E_t)^{1/2}$ (in rydbergs), where E_t is the target threshold energy and E is the continuum electron energy. In the region below each target threshold, the narrow autoionizing resonances are averaged using the Gailitis resonance-averaging procedure (Nahar & Pradhan 1991). The photoionization cross sections at higher photoelectron energies, beyond the highest target threshold, are extrapolated as explained in Nahar & Pradhan (1994). Illustrative examples of photoionization cross sections are given in Figures 1, 2, and 3 and are discussed in § 3.

2.3. *Total and State-specific Recombination Rate Coefficients*

The total and state-specific recombination rates coefficients are obtained using the unified treatment for both the RR and DR processes within the CC approximation using the ***R***-matrix method (Nahar & Pradhan 1994, 1995; Nahar 1996b). The infinite number of recombined states of the electron-ion system are divided into two groups according to their symmetries $nSL\pi$ as (1) low-n states, $n \leq n_0$, and (2) high-n states, $n_0 < n \leq \infty$, with $n_0 \sim 10$. The S, L, and π refer to the total spin, orbital angular momenta, and parity of the recombined state(s).

For electron-ion recombination to the low-n bound states of the first group, the recombination cross sections $\sigma_{\rm RC}$ and the recombination rate coefficients α_R are obtained from the detailed *partial* photoionization cross sections $\sigma_{\rm PI}$ through the Milne relation

$$\sigma_{\rm RC} = \sigma_{\rm PI}\,\frac{g_i}{g_j}\,\frac{h^2\omega^2}{4\pi^2m^2c^2v^2}\,. \tag{4}$$

where g_i and g_j are the statistical weight factors of the recombining and recombined ions, respectively, and v is the photoelectron velocity. Recombination rate coefficients of individual states are then obtained by averaging the recombination cross sections over the Maxwellian electron distribution $f(v)$ at a given temperature as

$$\alpha_{\rm RC}(T) = \int_0^\infty vf(v)\sigma_{\rm RC}\,dv\,, \tag{5}$$

With the sum of these individual rates providing the contributions of the low-n bound states to the total recombination rates (Nahar & Pradhan 1994),

$$\alpha_R(T;\, n \leq n_0) = \sum_j^{N_b}\frac{g_i}{g_j}\,\frac{2}{kTc^2\sqrt{2\pi m^3 kT}} \times \int_0^\infty E^2\sigma_{\rm PI}(j,\,\epsilon)e^{-\epsilon/kT}\,d\epsilon\,, \tag{6}$$

where $E = h\nu = \epsilon + I_P$, ϵ is the photoelectron energy, I_P is the ionization potential, and the sum is over partial recombination rates to bound states j, extending over the total number of bound states N_b. As the cross sections include the detailed structures of autoionizing resonances, equation (6) corresponds to the inclusion of RR and DR in a unified and ab initio manner for recombination to low-n states. A new computer program RECOMB is employed for the computations.

Recombination into the states of the second group ($n_0 < n \leq \infty$) with an excited core is dominated by DR via the high-n resonances; in this energy region, the background recombination via RR is small and may be neglected. The theory of DR developed by Bell & Seaton (1985; Nahar & Pradhan 1994; Nahar 1996b) is applied in order to compute the DR collision strengths Ω(DR) in this region. Transition probabilities for dipole-allowed transitions in the target ions are obtained from the oscillator strengths in the OP

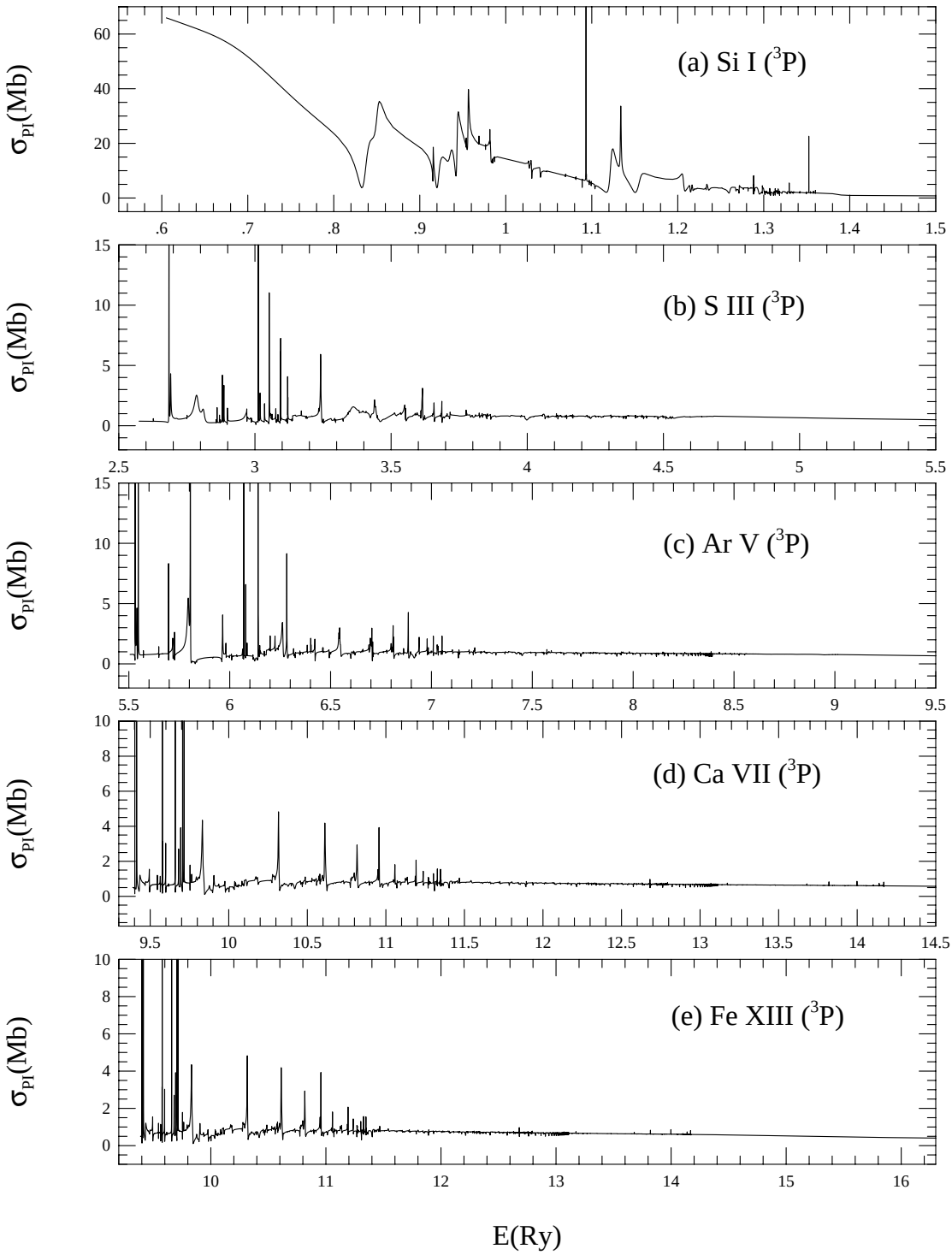

FIG. 1.—*Total* photoionization cross sections of the ground state $3s^2 3p^2(^3P)$ of Silicon-like ions: (*a*) Si I, (*b*) S III, (*c*) Ar V, (*d*) Ca VII, and (*e*) Fe XIII

database (C. Mendoza et al. 2000, in preparation) and are given in Table 2. Ω(DR) is obtained in the CC approximation using the same eigenfunction expansions as for the photoionization cross sections, with a new code STGFDR (Nahar & Pradhan 1994). The recombination cross sections are then

$$\sigma_{RC} = \frac{\pi}{g_i k^2}\,\Omega(\mathrm{DR})a_0^2\,, \qquad (7)$$

where k^2 is the energy of the electron. The rate coefficients are obtained from an averaged Maxwellian distribution. We calculate both the detailed and resonance-averaged forms of DR collision strength. However, the contributions to the total α_R are obtained from the resonance-averaged collision strength $\langle\Omega(\mathrm{DR})\rangle$.

Figures 4*a*, 4*b*, and 4*c* present the DR collision strengths Ω(DR) for Ar V, Ca VII, and Fe XIII, respectively, in the energy region below the excited target thresholds for dipole-

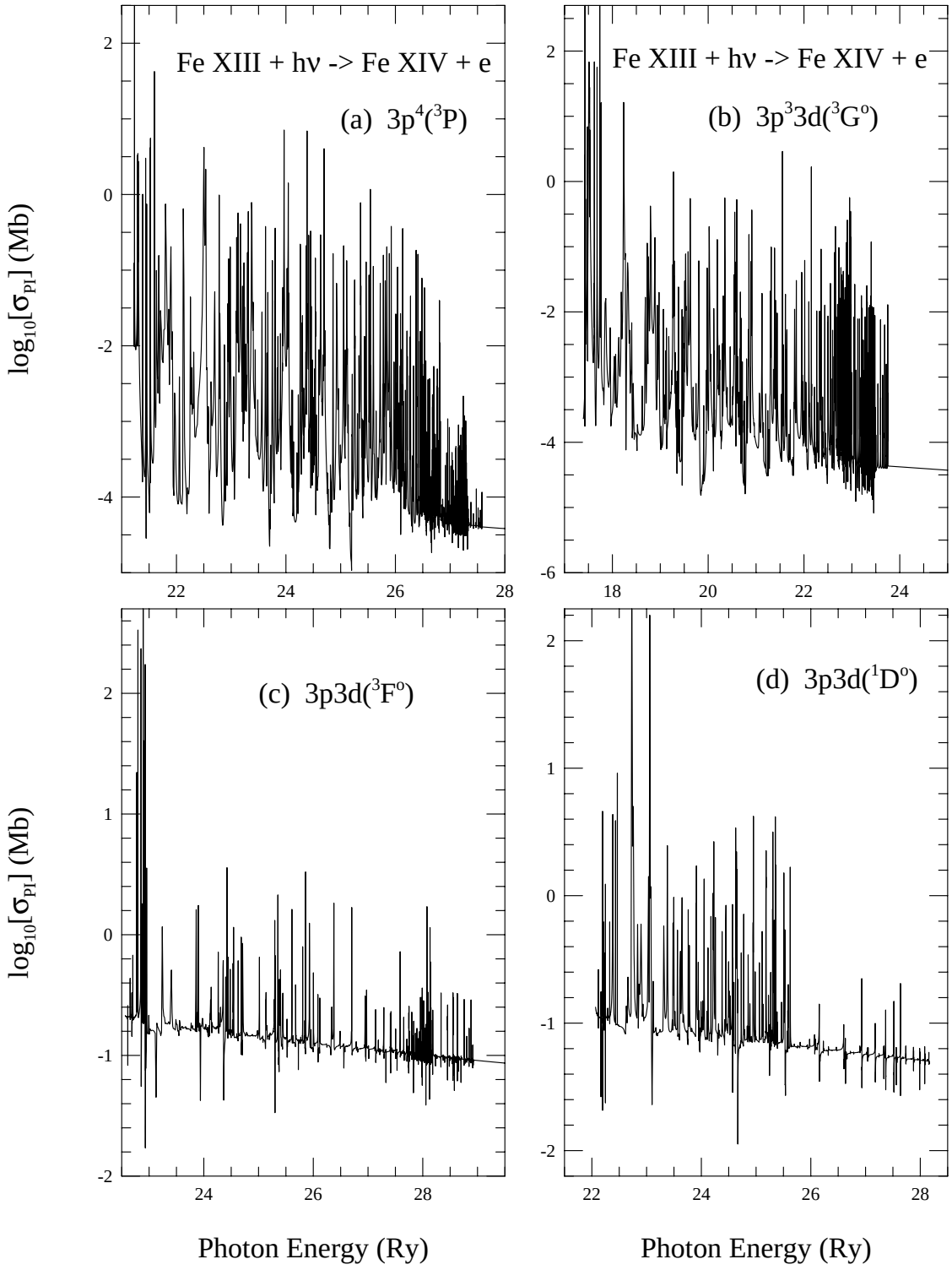

FIG. 2.—*Partial* photoionization cross sections of the bound states of Fe XIII: (*a*) $3p^4(^3P)$, (*b*) $3p^3 3d(^3G^o)$, (*c*) $3p3d(^3F^o)$, and (*d*) $3p3d(^1D^o)$

allowed transitions, relative to the target ground state $3p(^2P^o)$. Each plot has two panels; the lower one shows the expanded and detailed structures of Ω(DR), and the upper one shows the peak values as the resonances converge onto the respective thresholds. The dotted curves correspond to Ω(DR) with detailed resonance structures, while the solid curves are the resonance-averaged ones, ⟨Ω(DR)⟩. The features show the density increment of resonances, with effective quantum numbers, and the rise in background, indicating an increase in electron capture via the DR process as they approach the target threshold. At the threshold when the core ion is excited, DR goes to zero as the resonance-trapped flux is released into the electron impact excitation (EIE) channels. Therefore, the peak value of the resonance-averaged Ω(DR) at a threshold should be equal to the collision strength for electron impact excitation, Ω(EIE). Table 2 compares these two values at various thresholds (specified by arrows in the figures).

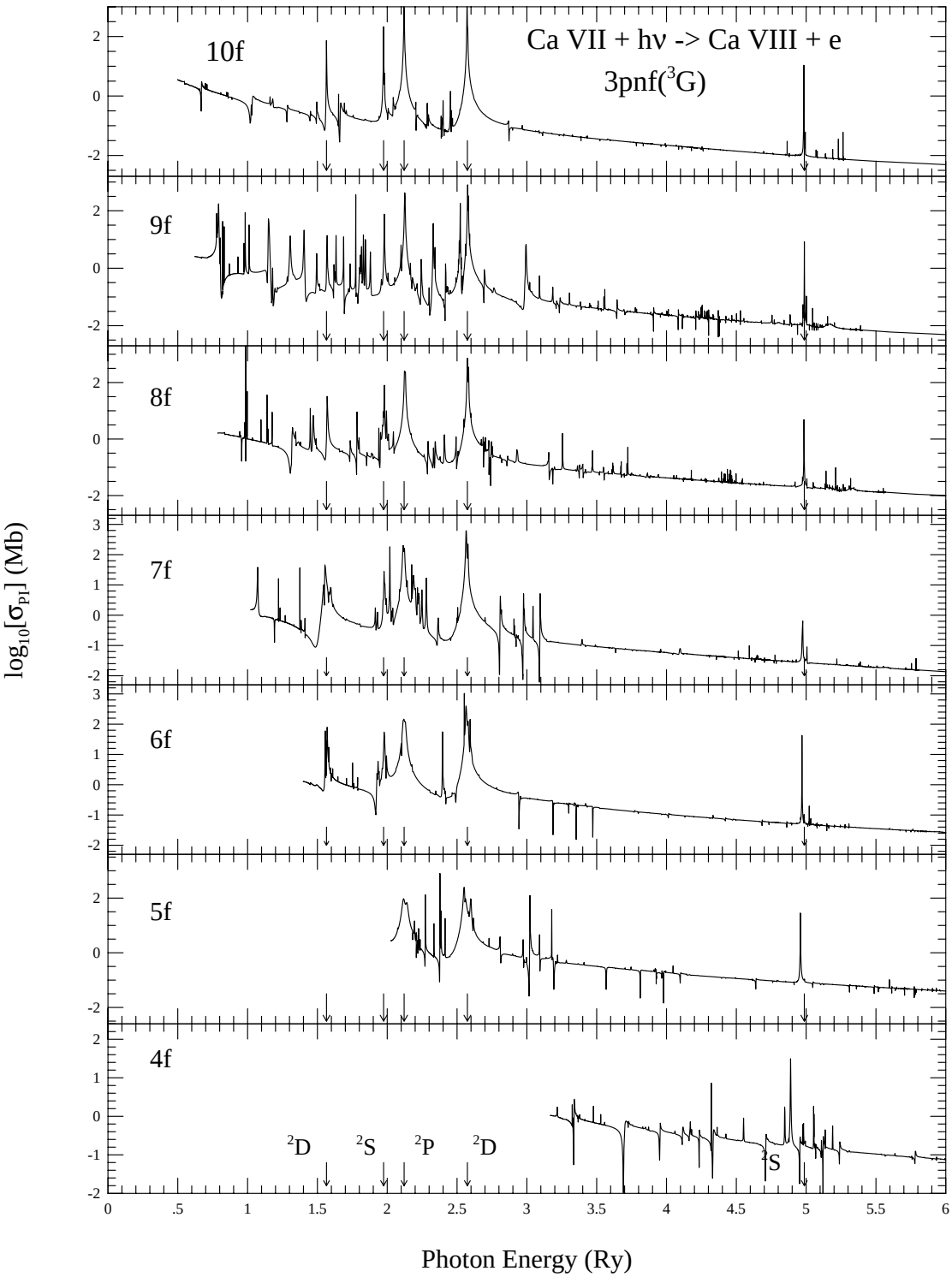

FIG. 3.—Partial photoionization cross sections of the states of Rydberg series, $3pnf(^3G)$, $4f \leq nf \leq 10f$, of Ca VII illustrating the PEC resonances. The arrows point to the PEC positions at threshold energies for dipole-allowed transitions from the core ground $3s^2 3p(^2P^o)$ state.

Ω(EIE) at the excited target thresholds are obtained independently through ***R***-matrix scattering calculations. These are shown in Figure 4 as well (*filled circles*). Values of Ω(EIE) are obtained in two ways: by excluding the contributions of perturbative multipole potentials (IP = 0) and by including them (IP = 1) in the asymptotic part of the wave functions (Nahar & Pradhan 1994), where IP is the switching parameter for these potentials in the code. The Bell & Seaton theory for DR does not include the contributions of these potentials. Hence, Ω(DR) should be compared with Ω(EIE) (IP = 0). Good agreement between the two sets of values is found in Table 2 and in Figure 4. Another purpose for calculating Ω(EIE) with IP = 0 and 1 is to find the importance of the contributions of the multipole potentials from the difference of the two. The nearly complete agreement between the two sets given in Table 2 implies negligi-

TABLE 2

TRANSITION PROBABILITIES AND COMPARISON OF COLLISION STRENGTHS[a]

TARGET STATE	A_{fi} (s^{-1})	$\langle\Omega(\mathrm{DR})\rangle$	Ω(EIE) IP = 0	Ω(EIE) IP = 1
Si II: $3s^23p\ ^2P^o$				
$3s3p^2(^2D)$.....	2.92(6)	3.91	5.88	5.88
$3s^24s(^2S)$	1.11(9)	0.448	0.448	0.506
$3s3p^2(^2S)$	1.08(9)	2.95	2.95	3.18
$3s^23d(^2D)$.....	2.95(9)	2.60	2.61	2.36
$3s3p^2(^2P)$.....	4.42(9)	0.782	0.782	0.81
S IV: $3s^23p\ ^2P^o$				
$3s3p^2(^2D)$.....	1.62(8)	10.71	9.88	9.91
$3s3p^2(^2S)$	3.30(9)	2.96	2.97	2.91
$3s3p^2(^2P)$.....	9.34(9)	15.82	15.88	15.63
$3s^23d(^2D)$.....	1.10(10)	12.70	12.53	13.50
$3s^24s(^2S)$	5.79(9)	0.719	0.725	0.759
Ar VI: $3s^23p\ ^2P^o$				
$3s3p^2(^2D)$.....	4.30(8)	6.57	6.51	6.19
$3s3p^2(^2S)$	5.08(9)	2.42	2.36	2.17
$3s3p^2(^2P)$.....	1.48(10)	16.10	16.07	15.43
$3s^23d(^2D)$.....	1.80(10)	12.38	12.33	12.60
$3s^24s(^2S)$	1.94(10)	0.191	0.191	0.189
Ca VIII: $3s^23p\ ^2P^o$				
$3s3p^2(^2D)$.....	7.57(8)	4.99	4.96	4.66
$3s3p^2(^2S)$	6.94(9)	4.74	4.602	4.115
$3s3p^2(^2P)$.....	2.03(10)	13.74	13.76	11.97
$3s^23d(^2D)$.....	2.20(10)	12.78	12.72	11.81
$3s^24s(^2S)$	4.59(10)	0.114	0.115	0.123
Fe XIV: $3s^23p\ ^2P^o$				
$3s3p^2(^2D)$.....	3.81(8)	3.67	3.75	3.26
$3s3p^2(^2S)$	8.89(9)	3.90	2.75	2.78
$3s3p^2(^2P)$.....	1.50(9)	7.51	7.53	7.07
$3s^23d(^2D)$.....	8.60(8)	7.12	7.31	6.49

[a] Transition probabilities A_{fi} to the ground $3s^23p(^2P^o)$ state and comparison of the DR collision strength $\langle\Omega(\mathrm{DR})\rangle$ with EIE collision strength Ω(EIE) at thresholds for dipole-allowed transitions of Si II–like target ions.

ble contributions from these potentials. This also indicates the convergence of the ***R***-matrix basis set within the ***R***-matrix boundary.

The "background" recombination (RR type) for the high-n states ($n_0 < n \leq \infty$) is usually negligibly small except at very low temperatures. Their contributions are obtained in the hydrogenic approximation, are included in the total recombination rate coefficients at all temperatures, and are referred to as the "top-up" part (Nahar 1996b). The rapid rise in α_R toward very low temperatures is due to low-energy recombination toward an infinite number of these high-n states where electron energies are not high enough for the target excitations.

3. RESULTS AND DISCUSSION

Photoionization and recombination rate coefficients are discussed separately in the following two subsections.

3.1. *Total and Partial Photoionization Cross Sections*

The *total* photoionization cross sections σ_{PI} for ionization into the ground and excited states of the core ion are obtained for all bound states N_b^T for each ion. The *total* cross sections are needed for various applications such as calculating opacities in plasmas and ionization fractions, while the *partial* ones are used for recombination rate coefficients.

Figure 1 presents the total σ_{PI} for the ground state $3s^23p^2(^3P)$ of Si-like ions. Except for the high resonances in the low-energy region, the background cross sections are featureless for all five ions. The wide resonance in the Si I cross sections is discussed in Nahar & Pradhan (1993). All ions show near-threshold resonances except S III. In the present calculations, the background cross sections of Ar V, Ca VII, and Fe XIII remain about the same as in the previous calculations (Nahar & Pradhan 1993; K. Butler et al. 2000, in preparation). The significant differences are seen for excited states because of the inclusion of more target states in the eigenfunction expansions.

The *partial* photoionization cross sections, for ionization into the ground state of the residual ion, are obtained for states that couple to the target ground state. The total and state-specific recombination rate coefficients of the ion are calculated from these cross sections. The total number of such bound states N_b that couple to the core ground state are usually less than the total number of bound states N_b^T.

Detailed structures of partial photoionization cross sections for a number of excited states relevant to the recombination rate coefficients are illustrated in Figures 2 and 3. Figure 2 presents σ_{PI} of excited states of Fe XIII. States with extensive resonances, such as $3p^4(^3P)$ (Fig. 2*a*) and $3p^33d(^3G^o)$ (Fig. 2*b*), usually dominate the recombination, especially in the low- and intermediate-temperature regions. The cross sections for these states usually decrease faster in the high-energy region. Some cross sections (e.g., those that are not densely populated with resonances) often dominate the recombination at high temperatures because of relatively higher background. Such examples are $3p3d(^3F^o)$ (Fig. 2*c*) and $3p3d(^1D^o)$ (Fig. 2*d*) of Fe XIII.

Figure 3 illustrates the departures from near-hydrogenic cross sections of excited states due to the larger number of relatively narrow resonances, along with comparatively wider resonances known as the photoexcitation of core (PEC) resonances in the high-energy region. PEC resonances occur at photon energies for dipole-allowed transitions in the core ion from its ground state. The process is essentially the inverse of DR; the outer Rydberg electron remains a "spectator," weakly interacting with the core ion, while the incident photon excites the dipole core transitions (Yu & Seaton 1987). Resonances with low effective quantum numbers contribute a relatively small amount to DR since their autoionization rates are usually orders of magnitude larger than the radiative decay rates. Radiative decays are more prominent at energies just below the threshold where PEC resonances occur. PEC resonance affects considerably the photoionization of excited bound states along a Rydberg series. Figure 3 presents photoionization cross sections of the Rydberg series of states, $3pnf(^3G)$, with $4f \leq nf \leq 10f$, of Ca VII. The arrows point to the positions of the core states (Table 1) for dipole-allowed transitions from the ground state $3s^23p(^2P^o)$ where the PEC resonances occur. These states contribute significantly at high temperatures.

3.2. *State-specific and Total Recombination Rate Coefficients*

The state-specific recombination rates are needed in the

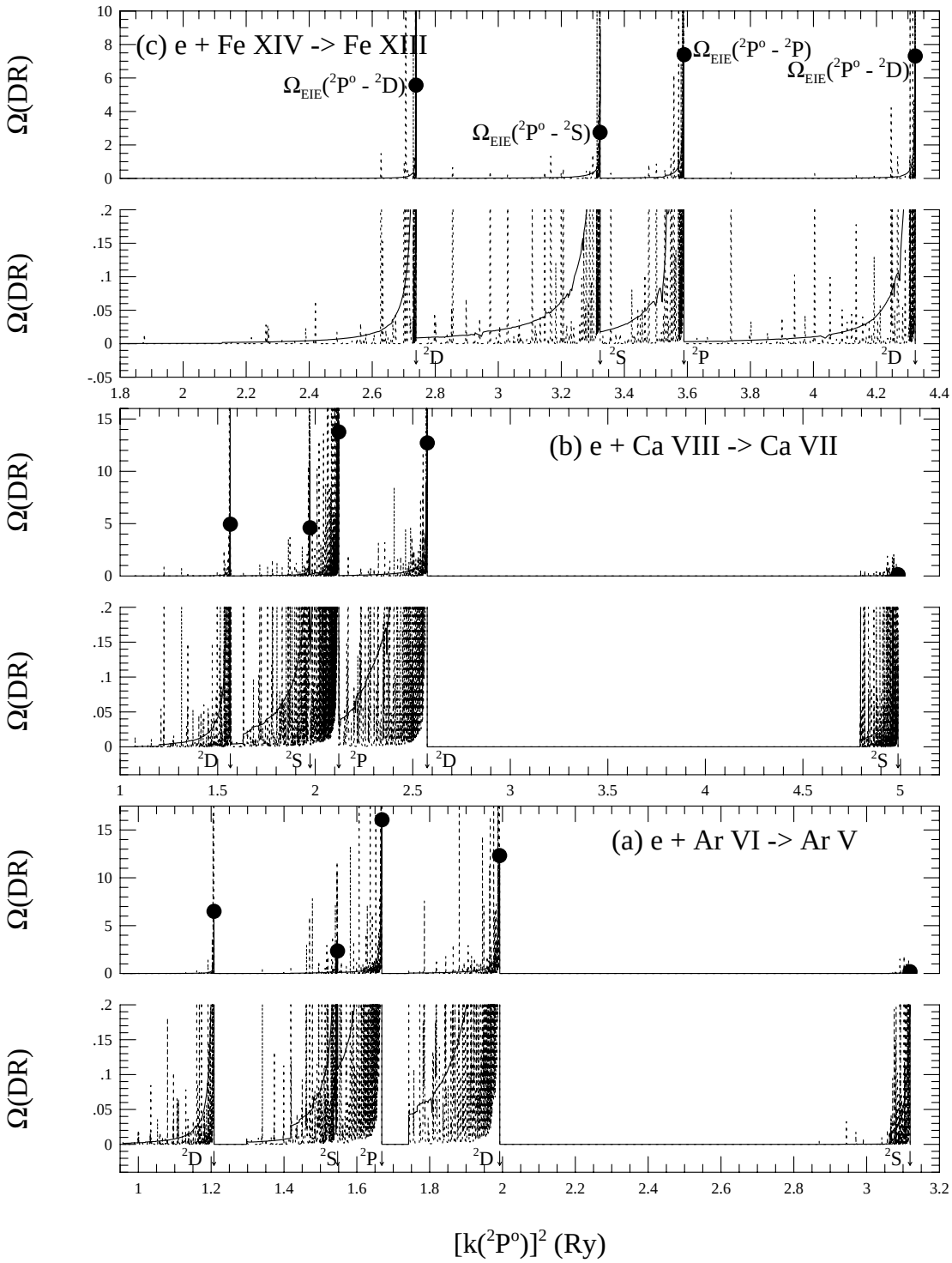

FIG. 4.—DR collision strengths Ω(DR) for (*a*) Ar V, (*b*) Ca VII, and (*c*) Fe XIII, detailed with resonances (*dotted curve*) and averaged over resonances (*solid curve*), in the regions below and at the excited thresholds (specified in the figures) for dipole-allowed transition from the ground state $^2P^o$. The filled circles are the calculated EIE collision strength, Ω_{EIE}, at the thresholds.

calculation of recombination line intensities; $\alpha_R(i \rightarrow j)$ gives a measure of the line intensity for the transition $i \rightarrow j$. Table 3 presents the state-specific, partial recombination rate coefficients of the 20 dominant low-n bound states of the first group at temperatures $T = 1000$, 10,000, 50,000, and 100,000 K. (The complete set of state-specific rate coefficients for a wide temperature range of all ions is available electronically.) The rates are listed in order of their percentage contributions to the total $\alpha_R(T)$ at these temperatures. Their sum shows that a limited number of states usually dominate the recombination rates at lower temperatures. For example, 20 states, out of 995, provide over a quarter of the contributions to the total α_R up to $T = 100{,}000$ K for Fe XIII. The number, the order, and the amount of the contribution of the individual bound states vary with temperature depending on the positions of the autoionizing

TABLE 3

STATE-SPECIFIC RECOMBINATION RATE COEFFICIENTS[a]

1000 K			10,000 K			50,000 K			100,000 K		
State		α_R	State		α_R	State		α_R	State		α_R
Si I: $N_b = 265$; $N_b^T = 266$											
$3s^23p^2$	$^3P^e$	$1.51-12$	$3s^23p^2$	$^3P^e$	$4.73-13$	$3s3p^2\ ^4P^e3d$	$^3D^e$	$2.02-13$	$3s3p^2\ ^4P^e3d$	$^3D^e$	$2.26-13$
$3s^23p^2$	$^1D^e$	$3.66-13$	$3s^23p^2$	$^1D^e$	$1.90-13$	$3s^23p^2$	$^3P^e$	$1.45-13$	$3p^4$	$^3P^e$	$1.10-13$
$3s^23p^2P^o4p$	$^3D^e$	$1.21-13$	$3s3p^2\ ^4P^e3d$	$^3D^e$	$8.99-14$	$3p^4$	$^3P^e$	$1.00-13$	$3s^23p^2P^o5p$	$^3D^e$	$7.53-14$
$3s^23p^2P^o3d$	$^3F^o$	$1.15-13$	$3s3p^2\ ^4P^e4f$	$^3G^o$	$4.67-14$	$3s^23p^2$	$^1D^e$	$9.38-14$	$3s^23p^2$	$^3P^e$	$7.18-14$
$3s^23p^2P^o4p$	$^3P^e$	$7.16-14$	$3s3p^2\ ^2D^e4f$	$^3H^o$	$4.52-14$	$3s3p^2\ ^2D^e4f$	$^3H^o$	$7.99-14$	$3s3p^2\ ^2D^e4f$	$^3H^o$	$6.87-14$
$3s3p^3$	$^3D^o$	$5.21-14$	$3p^4$	$^3P^e$	$3.95-14$	$3s^23p^2P^o5p$	$^3D^e$	$7.32-14$	$3s^23p^2P^o5p$	$^1D^e$	$6.20-14$
$3s^23p^2P^o5p$	$^3P^e$	$5.18-14$	$3s3p^3$	$^3D^o$	$3.82-14$	$3s^23p^2P^o4p$	$^3D^e$	$6.99-14$	$3s^23p^2P^o4p$	$^3D^e$	$6.13-14$
$3s^23p^2P^o4p$	$^1D^e$	$4.27-14$	$3s^23p^2P^o3d$	$^3F^o$	$3.69-14$	$3s3p^2\ ^4P^e4f$	$^3G^o$	$6.91-14$	$3s3p^2\ ^4P^e4f$	$^3G^o$	$5.88-14$
$3s^23p^2P^o5p$	$^3D^e$	$4.11-14$	$3s3p^2\ ^4P^e4f$	$^3F^o$	$3.00-14$	$3s3p^2\ ^4P^e4f$	$^3F^o$	$5.84-14$	$3p^4$	$^1D^e$	$5.83-14$
$3s^23p^2P^o3d$	$^1D^o$	$3.34-14$	$3s^23p^2P^o4p$	$^3D^e$	$2.18-14$	$3s^23p^2P^o5p$	$^1D^e$	$5.81-14$	$3s3p^2\ ^4P^e4f$	$^3F^o$	$5.37-14$
$3s^23p^2P^o3d$	$^3P^o$	$3.33-14$	$3s3p^2\ ^2D^e3d$	$^1P^e$	$2.09-14$	$3s^23p^2P^o3d$	$^3F^o$	$5.43-14$	$3s^23p^2P^o5p$	$^3P^e$	$5.24-14$
$3s^23p^2$	$^1S^e$	$3.23-14$	$3s^23p^2P^o5p$	$^3P^e$	$2.08-14$	$3p^4$	$^1D^e$	$5.27-14$	$3s^23p^2$	$^1D^e$	$5.17-14$
$3p^4$	$^3P^e$	$3.05-14$	$3s^23p^2P^o4p$	$^3P^e$	$2.06-14$	$3s^23p^2P^o5p$	$^3P^e$	$4.94-14$	$3s^23p^2P^o6f$	$^3D^e$	$4.65-14$
$3s^23p^2P^o4d$	$^3F^o$	$3.01-14$	$3s^23p^2P^o4d$	$^3D^o$	$1.81-14$	$3s^23p^2P^o4d$	$^3F^o$	$4.56-14$	$3s^23p^2P^o3d$	$^3F^o$	$4.52-14$
$3s^23p^2P^o5p$	$^1D^e$	$2.98-14$	$3s^23p^2$	$^1D^e$	$1.71-14$	$3s3p^3$	$^3D^o$	$4.53-14$	$3s^23p^2P^o4d$	$^3F^o$	$4.40-14$
$3s3p^2\ ^4P^e3d$	$^3D^e$	$2.07-14$	$3s^23p^2P^o5p$	$^3D^e$	$1.57-14$	$3s^23p^2P^o6f$	$^3D^e$	$4.45-14$	$3s3p^2\ ^2D^e3d$	$^1P^e$	$4.10-14$
$3s^23p^2P^o6h$	$^3I^e$	$1.72-14$	$3s3p^2\ ^2D^e4f$	$^1G^o$	$1.55-14$	$3s^23p^2P^o4p$	$^3P^e$	$4.04-14$	$3s3p^2\ ^2D^e3d$	$^3S^e$	$3.96-14$
$3s^23p^2P^o7h$	$^3I^e$	$1.57-14$	$3s3p^2\ ^2D^e4f$	$^1H^o$	$1.51-14$	$3s3p^2\ ^2D^e3d$	$^1P^e$	$3.95-14$	$3s^23p^2P^o10d$	$^1F^o$	$3.79-14$
$3s^23p^2P^o5p$	$^3S^e$	$1.57-14$	$3s3p^2\ ^2D^e3d$	$^3S^e$	$1.34-14$	$3s3p^2\ ^2D^e3d$	$^3S^e$	$3.44-14$	$3s^23p^2P^o10d$	$^1F^o$	$3.79-14$
$3s^23p^2P^o6h$	$^3H^e$	$1.45-14$	$3s^23p^2$	$^1S^e$	$1.33-14$	$3s^23p^2P^o5p$	$^1P^e$	$3.33-14$	$3s^23p^2P^o4p$	$^3P^e$	$3.51-14$
Sum		$2.65-12$			$1.18-12$			$1.39-12$			$1.28-12$
Total		$3.72-12$			$1.60-12$			$7.97-12$			$8.24-12$
Contribution (%).....		71			74			17			16
S III: $N_b = 298$; $N_b^T = 309$											
$3s^23p^2P^o3d$	$^3P^o$	$1.09-11$	$3s^23p^2P^o3d$	$^3D^o$	$2.66-12$	$3s^23p^2P^o3d$	$^3D^o$	$1.17-12$	$3s^23p^2P^o3d$	$^3D^o$	$5.66-13$
$3s^23p^2P^o3d$	$^3F^o$	$4.71-12$	$3s^23p^2P^o3d$	$^3F^o$	$1.85-12$	$3s^23p^2P^o3d$	$^3P^o$	$5.61-13$	$3s^23p^2P^o4p$	$^3D^e$	$3.13-13$
$3s3p^3$	$^3S^o$	$4.52-12$	$3s^23p^2P^o3d$	$^3P^o$	$1.62-12$	$3s^23p^2P^o3d$	$^3F^o$	$5.58-13$	$3s^23p^2P^o3d$	$^3F^o$	$2.97-13$
$3s^23p^2P^o4s$	$^3P^o$	$4.26-12$	$3s3p^3$	$^3S^o$	$1.35-12$	$3s^23p^2P^o4p$	$^3D^e$	$5.40-13$	$3s^23p^2P^o4d$	$^3F^o$	$2.94-13$
$3s^23p^2P^o3d$	$^1D^o$	$2.52-12$	$3s^23p^2P^o3d$	$^1D^o$	$1.11-12$	$3s^23p^2P^o3d$	$^1F^o$	$4.94-13$	$3s^23p^2P^o9h$	$^3I^e$	$2.75-13$
$3s3p^3$	$^1P^o$	$2.43-12$	$3s^23p^2P^o4s$	$^3P^o$	$9.29-13$	$3s3p^2\ ^4P^e3d$	$^3F^e$	$4.00-13$	$3s^23p^2P^o8h$	$^3H^e$	$2.66-13$
$3s3p^3$	$^3P^o$	$1.54-12$	$3s^23p^2P^o3d$	$^1F^o$	$8.96-13$	$3s^23p^2P^o3d$	$^1D^o$	$3.92-13$	$3s^23p^2P^o3d$	$^3P^o$	$2.62-13$
$3s^23p^2P^o4s$	$^1P^o$	$1.42-12$	$3s3p^3$	$^3P^o$	$7.14-13$	$3s^23p^2P^o4s$	$^3P^o$	$3.89-13$	$3s3p^2\ ^4P^e3d$	$^3F^e$	$2.55-13$
$3s3p^3$	$^1D^o$	$1.40-12$	$3s3p^3$	$^1P^o$	$5.63-13$	$3s^23p^2P^o4d$	$^3F^o$	$3.20-13$	$3s^23p^2P^o6h$	$^3I^e$	$2.54-13$
$3s3p^3$	$^3D^o$	$1.19-12$	$3s^23p^2P^o4s$	$^1P^o$	$5.33-13$	$3s^23p^2P^o4p$	$^3P^e$	$3.04-13$	$3s^23p^2P^o3d$	$^1F^o$	$2.53-13$
$3s^23p^2P^o3d$	$^1F^o$	$1.15-12$	$3s3p^2\ ^4P^e3d$	$^3F^e$	$4.53-13$	$3s3p^3$	$^3S^o$	$2.99-13$	$3s^23p^2P^o5g$	$^3H^o$	$2.43-13$
$3s^23p^2P^o3d$	$^3D^o$	$3.71-13$	$3s3p^3$	$^3D^o$	$3.88-13$	$3p^4$	$^3P^e$	$2.65-13$	$3s^23p^2P^o6h$	$^3G^e$	$2.28-13$
$3s^23p^2P^o4d$	$^3F^o$	$3.18-13$	$3s3p^2\ ^2D^e3d$	$^3F^e$	$3.52-13$	$3s^23p^2P^o4d$	$^3D^o$	$2.24-13$	$3s^23p^2P^o4d$	$^3D^o$	$2.19-13$
$3s^23p^2P^o4d$	$^3D^o$	$2.55-13$	$3s3p^3$	$^1D^o$	$3.29-13$	$3s^23p^2P^o4f$	$^3G^e$	$2.09-13$	$3s^23p^2P^o4f$	$^3G^e$	$1.98-13$
$3s^23p^2P^o4f$	$^3G^e$	$2.12-13$	$3s^23p^2P^o4p$	$^3D^e$	$3.06-13$	$3s3p^2\ ^2D^e3d$	$^3G^e$	$1.99-13$	$3s3p^2\ ^2D^e3d$	$^3G^e$	$1.96-13$
$3s3p^2\ ^4P^e4p$	$^3P^o$	$1.97-13$	$3s^23p^2P^o4p$	$^3P^e$	$1.51-13$	$3s^23p^2P^o6h$	$^3I^e$	$1.78-13$	$3s^23p^2P^o4s$	$^3P^o$	$1.91-13$
$3s^23p^2P^o4d$	$^3P^o$	$1.69-13$	$3s^23p^2P^o3d$	$^1P^o$	$1.37-13$	$3s^23p^2P^o3d$	$^1P^o$	$1.66-13$	$3s^23p^2P^o3d$	$^1D^o$	$1.90-13$
$3s^23p^2P^o5d$	$^3D^o$	$1.69-13$	$3s3p^2\ ^4P^e4p$	$^3P^o$	$1.37-13$	$3s^23p^2P^o5g$	$^3H^o$	$1.61-13$	$3s^23p^2P^o4p$	$^3P^e$	$1.88-13$
$3s^23p^2$	$^3P^e$	$1.55-13$	$3s3p^2\ ^4P^e4p$	$^3D^o$	$1.15-13$	$3s^23p^2P^o4s$	$^1P^o$	$1.60-13$	$3p^4$	$^3P^e$	$1.80-13$
$3s^23p^2P^o5d$	$^3F^o$	$1.43-13$	$3s^23p^2P^o4d$	$^3P^o$	$1.11-13$	$3s^23p^2P^o4p$	$^1D^e$	$1.55-13$	$3s^23p^2P^o6g$	$^3H^o$	$1.71-13$
Sum		$3.80-11$			$1.46-11$			$7.15-12$			$5.04-12$
Total		$5.23-11$			$1.81-11$			$5.26-11$			$1.09-10$
Contribution (%).....		73			81			14			5
Ar V: $N_b = 396$; $N_b^T = 581$											
$3s3p^2\ ^2P^e3d$	$^3F^e$	$1.08-11$	$3s3p^2\ ^2P^e3d$	$^3F^e$	$1.64-11$	$3s3p^2\ ^2P^e3d$	$^3F^e$	$3.09-12$	$3s3p^2\ ^2P^e3d$	$^3F^e$	$1.35-12$
$3s3p^2\ ^2D^e3d$	$^1F^e$	$8.14-12$	$3s^23d^2D^e3d$	$^3F^e$	$4.82-12$	$3s^23p^2P^o4f$	$^3G^e$	$1.75-12$	$3s^23p^2P^o4f$	$^3G^e$	$9.37-13$
$3s^23p^2P^o4f$	$^1G^e$	$6.12-12$	$3s3p^2\ ^2P^e3d$	$^3D^e$	$3.91-12$	$3s^23d^2D^e3d$	$^3F^e$	$1.50-12$	$3s^23p^2P^o4f$	$^3F^e$	$9.30-13$
$3s3p^2\ ^2D^e3d$	$^1S^e$	$4.30-12$	$3s^23p^2P^o4d$	$^3F^o$	$3.88-12$	$3s^23p^2P^o4f$	$^3F^e$	$1.44-12$	$3s^23d^2D^e3d$	$^3F^e$	$8.07-13$
$3s^23p^2P^o3d$	$^3F^o$	$4.05-12$	$3s3p^2\ ^2S^e3d$	$^3D^e$	$3.69-12$	$3s^23p^2P^o4d$	$^3F^o$	$1.41-12$	$3s3p^2\ ^2P^e3d$	$^3D^e$	$6.63-13$
$3s3p^2\ ^2S^e3d$	$^3D^e$	$3.96-12$	$3s^23p^2P^o4f$	$^3G^e$	$3.22-12$	$3s3p^2\ ^2P^e3d$	$^3D^e$	$1.36-12$	$3s^23p^2P^o4d$	$^3F^o$	$6.37-13$
$3s3p^2\ ^2P^e3d$	$^1F^e$	$3.71-12$	$3s3p^2\ ^2D^e3d$	$^3F^e$	$2.96-12$	$3s^23p^2P^o4f$	$^3D^e$	$1.02-12$	$3s^23p^2P^o4f$	$^3D^e$	$5.50-13$
$3s^23p^2P^o4f$	$^1F^e$	$3.24-12$	$3s^23p^2P^o4d$	$^3D^o$	$2.13-12$	$3s3p^2\ ^2S^e3d$	$^3D^e$	$9.89-13$	$3s3p^2\ ^2D^e3d$	$^3G^e$	$5.45-13$
$3s3p^2\ ^2S^e3d$	$^1D^e$	$2.90-12$	$3s^23p^2P^o4f$	$^3F^e$	$2.08-12$	$3s^23p^2P^o4d$	$^3D^o$	$9.64-13$	$3s^23p^2P^o3d$	$^3F^o$	$5.38-13$
$3s^23p^2P^o3d$	$^3D^o$	$2.79-12$	$3s^23p^2P^o4f$	$^3D^e$	$1.92-12$	$3s3p^2\ ^2D^e3d$	$^3F^e$	$9.15-13$	$3s3p^2\ ^2S^e3d$	$^3D^e$	$5.00-13$
$3s3p^2\ ^2D^e3d$	$^1D^e$	$2.50-12$	$3s3p^2\ ^2P^e3d$	$^1F^e$	$1.75-12$	$3s3p^2\ ^2D^e3d$	$^3G^e$	$8.84-13$	$3s^23p^2P^o4d$	$^3D^o$	$4.60-13$

TABLE 3—*Continued*

1000 K			10,000 K			50,000 K			100,000 K		
State		α_R	State		α_R	State		α_R	State		α_R
$3s3p^2\ ^2D^e3d$	$^1P^e$	2.36−12	$3s^23p^2P^o4f$	$^1G^e$	1.66−12	$3s^23p^2P^o3d$	$^3F^o$	8.42−13	$3s3p^2\ ^2D^e3d$	$^3F^e$	4.54−13
$3s^23p^2P^o4f$	$^3G^e$	2.23−12	$3s3p^2\ ^2D^e3d$	$^3D^e$	1.62−12	$3s3p^2\ ^4P^e4s$	$^3P^e$	7.20−13	$3s^23p^2P^o5g$	$^3H^o$	4.46−13
$3s3p^2\ ^2P^e3d$	$^1P^e$	1.96−12	$3s3p^2\ ^2D^e3d$	$^1F^e$	1.61−12	$3s3p^2\ ^2P^e3d$	$^3P^e$	7.05−13	$3s3p^2\ ^2P^e3d$	$^3P^e$	4.18−13
$3s^23p^2$	$^3P^e$	1.86−12	$3s^23p^2P^o3d$	$^3F^o$	1.50−12	$3s3p^2\ ^2P^e3d$	$^1F^e$	6.60−13	$3s^23p^2P^o4f$	$^3G^e$	4.09−13
$3s^23d^2D^e3d$	$^3F^e$	1.74−12	$3s3p^2\ ^2S^e3d$	$^1D^e$	1.30−12	$3s3p^2\ ^4P^e3d$	$^3F^e$	6.35−13	$3s^23d^2$	$^1G^e$	3.72−13
$3s3p^2\ ^2P^e3d$	$^3D^e$	1.66−12	$3s3p^2\ ^4P^e4s$	$^3P^e$	1.18−12	$3s3p^2\ ^2D^e3d$	$^3D^e$	6.15−13	$3s3p^2\ ^4P^e4s$	$^3P^e$	3.61−13
$3s^23p^2P^o3d$	$^1F^o$	1.57−12	$3s3p^2\ ^2D^e3d$	$^1P^e$	1.17−12	$3s^23p^2P^o4d$	$^3P^o$	5.51−13	$3s^23p^2P^o5p$	$^3D^e$	3.55−13
$3s^23p^2P^o3d$	$^3P^o$	1.46−12	$3s^23p^2P^o4d$	$^3P^o$	1.15−12	$3s^23p^2P^o4f$	$^1F^e$	5.45−13	$3s^23p^2P^o4f$	$^1F^e$	3.52−13
$3s3p^2\ ^2D^e3d$	$^1G^e$	1.38−12	$3s3p^2\ ^2D^e3d$	$^3P^e$	1.14−12	$3s^23p^2P^o5p$	$^3D^e$	5.16−13	$3s3p^2\ ^2P^e3d$	$^1F^e$	3.51−13
Sum		6.87−11			5.91−11			2.11−11			1.14−11
Total		1.32−10			9.18−11			7.10−11			1.46−10
Contribution (%).....		52			64			30			8.%
Ca VII: $N_b = 553$; $N_b^T = 631$											
$3s3p^3$	$^1D^o$	7.32−11	$3s^23p^2P^o5p$	$^3D^e$	1.02−11	$3s3p^2\ ^2P^e3d$	$^3F^e$	2.60−12	$3s3p^2\ ^2P^e3d$	$^3F^e$	1.31−12
$3s^23p^2$	$^3P^e$	2.54−11	$3s3p^2\ ^2P^e3d$	$^3F^e$	9.25−12	$3s^23p^2P^o5g$	$^3H^o$	2.09−12	$3s^23p^2P^o5g$	$^3H^o$	1.27−12
$3s3p^2\ ^4P^e3d$	$^3F^e$	2.06−11	$3s^23p^2P^o5p$	$^3P^e$	6.55−12	$3s^23p^2P^o4d$	$^3F^o$	2.07−12	$3s3p3d^2$	$^3F^o$	1.25−12
$3s3p^2\ ^2P^e3d$	$^3F^e$	1.73−11	$3s^23p^2$	$^3P^e$	6.18−12	$3s3p^2\ ^2D^e3d$	$^3F^e$	1.96−12	$3s^23p^2P^o4d$	$^3F^o$	1.14−12
$3p^33d$	$^1F^o$	1.68−11	$3s3p^2\ ^2D^e3d$	$^3F^e$	5.50−12	$3s3p3d^2$	$^3F^o$	1.93−12	$3s^23p^2P^o5f$	$^3G^e$	1.11−12
$3s3p^2\ ^2D^e3d$	$^3F^e$	1.65−11	$3s3p^2\ ^4P^e3d$	$^3F^e$	5.48−12	$3s^23p^2P^o5f$	$^3G^e$	1.91−12	$3s3p^2\ ^2D^e3d$	$^3F^e$	1.08−12
$3s^23d^2D^e4p$	$^1D^o$	1.54−11	$3s3p^3$	$^1D^o$	4.41−12	$3s3p^2\ ^4P^e3d$	$^3F^e$	1.73−12	$3s3p^2\ ^2D^e3d$	$^3G^e$	1.07−12
$3s3p3d^2$	$^1F^o$	1.44−11	$3s3p^2\ ^2S^e3d$	$^3D^e$	4.25−12	$3s^23p^2P^o5p$	$^3D^e$	1.68−12	$3s^23d^2$	$^3F^e$	1.04−12
$3s3p3d^2$	$^3F^o$	1.27−11	$3s^23p^2P^o5f$	$^3G^e$	4.00−12	$3s^23p^2P^o5f$	$^3F^e$	1.58−12	$3s3p3d^2$	$^3G^o$	9.85−13
$3s3p^2\ ^2D^e3d$	$^3D^e$	1.18−11	$3s^23p^2P^o5f$	$^3F^e$	3.66−12	$3s3p^2\ ^2D^e3d$	$^3G^e$	1.39−12	$3s^23p^2P^o5g$	$^3G^o$	9.71−13
$3s^23p^2P^o4s$	$^1P^o$	1.17−11	$3s3p^2\ ^2P^e3d$	$^3D^e$	3.44−12	$3s^23p^2P^o5g$	$^3G^o$	1.39−12	$3s3p^2\ ^4P^e3d$	$^3F^e$	9.29−13
$3s^23d^2$	$^3F^e$	1.13−11	$3s^23d^2$	$^3F^e$	3.44−12	$3s^23d^2$	$^3F^e$	1.32−12	$3s^23p^2P^o3d$	$^3F^o$	8.86−13
$3s3p^2\ ^2S^e3d$	$^3D^e$	1.01−11	$3s3p^2\ ^2D^e3d$	$^3D^e$	3.38−12	$3s^23p^2P^o3d$	$^3F^o$	1.30−12	$3s^23p^2P^o5f$	$^3F^e$	8.78−13
$3s3p^2\ ^2P^e3d$	$^3D^e$	9.74−12	$3s3p^2\ ^2P^e3d$	$^3P^e$	3.12−12	$3s3p^2\ ^2S^e3d$	$^3D^e$	1.29−12	$3s3p^2\ ^2D^e4p$	$^3F^o$	8.11−13
$3p^3\ ^2D^o3d$	$^1D^o$	8.27−12	$3s^23p^2P^o5g$	$^3H^o$	2.80−12	$3p^3\ ^2D^o3d$	$^3D^o$	1.24−12	$3s3p^2\ ^2D^e4d$	$^3G^e$	7.82−13
$3s3p^2\ ^4P^e3d$	$^3D^e$	7.09−12	$3s3p^3$	$^3D^o$	2.47−12	$3s3p3d^2$	$^3G^o$	1.21−12	$3s3p^2\ ^4P^e4f$	$^3G^o$	7.06−13
$3s3p3d^2$	$^1F^o$	6.76−12	$3s^23p^2P^o4s$	$^1P^o$	2.37−12	$3s3p^2\ ^2D^e3d$	$^3D^e$	1.21−12	$3s3p^2\ ^2S^e3d$	$^3D^e$	7.04−13
$3p^3\ ^2D^o3d$	$^1F^o$	6.47−12	$3s^23p^2P^o3d$	$^3F^o$	2.32−12	$3s3p^2\ ^2P^e3d$	$^3D^e$	1.20−12	$3s^23p^2$	$^1D^e$	7.04−13
$3s3p3d^2$	$^1F^o$	6.43−12	$3s^23p^2P^o5p$	$^1D^e$	2.19−12	$3s^23p^2$	$^3P^e$	1.17−12	$3s3p^2\ ^2D^e3d$	$^3D^e$	6.84−13
$3s^23p^2P^o3d$	$^3F^o$	6.09−12	$3s3p^2\ ^4P^e3d$	$^3D^e$	2.12−12	$3s3p^2\ ^4P^e4d$	$^3F^e$	1.17−12	$3p^3\ ^2D^o3d$	$^3D^o$	6.74−13
Sum		3.08−10			8.71−11			3.14−11			1.90−11
Total		5.90−10			1.90−10			1.22−10			1.85−10
Contribution (%).....		52			46			26			10
Fe XIII: $N_b = 995$; $N_b^T = 1223$											
$3s3p^2\ ^2P^e3d$	$^1F^e$	1.12−10	$3s3p^2\ ^4P^e3d$	$^3F^e$	3.43−11	$3p^3\ ^2D^o3d$	$^3G^o$	1.23−11	$3s^23p^2P^o3d$	$^1D^o$	9.49−12
$3s3p^2\ ^4P^e3d$	$^3F^e$	7.15−11	$3p^3\ ^2D^o3d$	$^3G^o$	3.32−11	$3s^23p^2P^o3d$	$^1D^o$	9.10−12	$3p^3\ ^2D^o3d$	$^3G^o$	5.72−12
$3p^4$	$^3P^e$	5.99−11	$3s3p^2\ ^2D^e3d$	$^3G^e$	3.11−11	$3p^3\ ^2D^o3d$	$^3F^o$	7.81−12	$3s^23p^2P^o3d$	$^1F^o$	4.58−12
$3s3p^2\ ^4P^e3d$	$^3P^e$	5.35−11	$3s3p^2\ ^2P^e3d$	$^3F^e$	2.69−11	$3s3p^2\ ^2P^e3d$	$^3F^e$	6.48−12	$3s3p3d^2$	$^3F^o$	4.57−12
$3s3p^2\ ^4P^e4d$	$^3F^e$	4.05−11	$3s3p^2\ ^2D^e3d$	$^3F^e$	2.34−11	$3s^23p^2P^o3d$	$^3F^o$	5.81−12	$3p^3\ ^2D^o3d$	$^3F^o$	3.94−12
$3s3p^2\ ^2D^e3d$	$^3F^e$	3.40−11	$3p^3\ ^2D^o3d$	$^3F^o$	1.62−11	$3s3p^2\ ^2D^e3d$	$^3G^e$	5.75−12	$3s^23p^2P^o3d$	$^3F^o$	3.62−12
$3s3p^2\ ^2D^e3d$	$^3P^e$	3.34−11	$3s3p^2\ ^2D^e3d$	$^3D^e$	1.47−11	$3s^23p^2P^o7i$	$^3K^o$	5.12−12	$3s3p3d^2$	$^3G^o$	3.50−12
$3s3p^2\ ^4P^e3d$	$^3D^e$	2.65−11	$3s3p^2\ ^2S^e3d$	$^3D^e$	1.34−11	$3s3p^2\ ^4P^e3d$	$^3F^e$	4.96−12	$3s^23p^2P^o7i$	$^3K^o$	3.40−12
$3s^23d^2D^e4s$	$^1D^e$	2.32−11	$3s3p^2\ ^4P^e3d$	$^3D^e$	1.33−11	$3s3p3d^2$	$^3G^o$	4.80−12	$3s3p^2\ ^2P^e3d$	$^3F^e$	3.39−12
$3s3p^2\ ^2P^e3d$	$^1D^e$	2.15−11	$3s^23p^2P^o7f$	$^3G^e$	1.31−11	$3s^23p^2P^o3d$	$^1F^o$	4.80−12	$3s3p3d^2$	$^3G^o$	3.06−12
$3s3p^2\ ^4P^e4d$	$^3D^e$	2.11−11	$3s3p^2\ ^2P^e3d$	$^1F^e$	1.17−11	$3s3p3d^2$	$^3F^o$	4.71−12	$3s3p^2\ ^2D^e3d$	$^3G^e$	2.47−12
$3p^23d^2$	$^1G^e$	1.61−11	$3s3p^2\ ^2P^e3d$	$^3P^e$	1.10−11	$3p^3\ ^2D^o3d$	$^3P^o$	4.31−12	$3s^23p^2P^o7h$	$^3I^e$	2.46−12
$3s3p^2\ ^4P^e4d$	$^3P^e$	1.58−11	$3s3p^2\ ^2D^e3d$	$^3P^e$	1.09−11	$3s^23p^2P^o7h$	$^3I^e$	4.14−12	$3s^23d^2$	$^3P^e$	2.37−12
$3s^23p^2P^o3d$	$^3F^o$	1.56−11	$3s3p^2\ ^4P^e3d$	$^3P^e$	1.07−11	$3s3p^2\ ^2D^e3d$	$^3F^e$	4.10−12	$3p^3\ ^2D^o3d$	$^3P^o$	2.33−12
$3s^23d^2$	$^1G^e$	1.50−11	$3p^3\ ^2D^o4d$	$^3G^o$	1.07−11	$3p^3\ ^2D^o3d$	$^1G^o$	3.73−12	$3s3p^2\ ^4P^e3d$	$^3F^e$	2.13−12
$3s^23p^2$	$^3P^e$	1.44−11	$3s^23p^2P^o7f$	$^3F^e$	1.06−11	$3s3p^2\ ^2S^e3d$	$^3D^e$	3.69−12	$3s3p^2\ ^2S^e3d$	$^3D^e$	2.05−12
$3p^4$	$^1D^e$	1.38−11	$3s3p^2\ ^2D^e4d$	$^3G^e$	9.93−12	$3s^23p^2P^o7g$	$^3H^o$	3.58−12	$3s3p^2\ ^2D^e3d$	$^3F^e$	2.02−12
$3s3p^2\ ^4P^e5d$	$^3F^e$	1.37−11	$3s3p^2\ ^4P^e4d$	$^3F^e$	9.92−12	$3s3p3d^2$	$^3G^o$	3.56−12	$3p^3\ ^2D^o3d$	$^3D^o$	2.02−12
$3s^23d^2$	$^1D^e$	1.28−11	$3s3p^2\ ^2P^e3d$	$^3D^e$	9.56−12	$3p^3\ ^2D^o4d$	$^3G^o$	3.44−12	$3s^23p^2P^o7g$	$^3H^o$	1.99−12
$3s3p^2\ ^2D^e3d$	$^3D^e$	1.15−11	$3p^3\ ^2D^o3d$	$^1G^o$	9.48−12	$3s^23p^2P^o7f$	$^3G^e$	3.34−12	$3p^3\ ^2D^o3d$	$^1G^o$	1.90−12
Sum		6.26−10			3.24−10			1.06−10			6.70−11
Total		1.38E−09			9.68−10			3.88−10			2.59−10
Contribution		46			34			27			26

[a] Coefficients are given (in units of $cm^3\ s^{-1}$) for the dominant 20 states of Si I, S III, Ar V, Ca VII, and Fe XIII, in order of their contributions to the total α_R at temperatures $T = 1000$, 10,000, 500,00, and 100,000 K. N_b is the number of bound states for which state-specific rates are obtained, and N_b^T is the number of total bound states of the ion.

resonances in the cross sections. The ground state may not necessarily be the dominant contributor at all temperatures. The state-specific recombination rates given for all ions should be close to their total recombination rate coefficients at these temperatures, except for Si I at 100,000 K. The incident electron energies at these temperatures lie well below the first excited target threshold for a dipole-allowed transition except for Si I. At higher temperatures, the state-specific rates may have been underestimated since the high-n DR contributions are not included in them individually.

The total recombination rate coefficients $\alpha_R(T)$ are computed over a wide range of temperatures, $1 \leq \log_{10} T \leq 8$, at a fine temperature mesh $\Delta T = 0.1$ for easy interpolation. The values are given in Table 4, and the features of total $\alpha_R(T)$ are shown in Figures 5*a*–5*c* (*solid curves*). Each figure has two panels: the top panel shows the rates over a wide range of temperatures, while the bottom panel presents an expanded part of the temperature range where the rates go through a minimum before being dominated by the DR process. Starting with high recombination at very low temperature, the rate coefficient decreases until it reaches a minimum and then it peaks at high temperature (for example, at $\log_{10} T = 5.2$ K for Ar V), because of the dominance of DR followed by a decay at higher temperatures. Owing to near-threshold autoionizing resonances in photoionization cross sections, the recombination rate may also exhibit a low-temperature bump (e.g., Nussbaumer & Storey 1983; Nahar & Pradhan 1994). All three ions, Ar V, Ca VII, and Fe XIII, show such low-temperature bumps.

Comparisons of the present $\alpha_R(T)$ with the previous ones are made in Figures 5*a*–5*c*. As mentioned above, the solid curves are the present unified *total* recombination rate coefficients. In the bottom panel of each figure, the dotted curve is the sum of RR and DR rates from previous calculations.

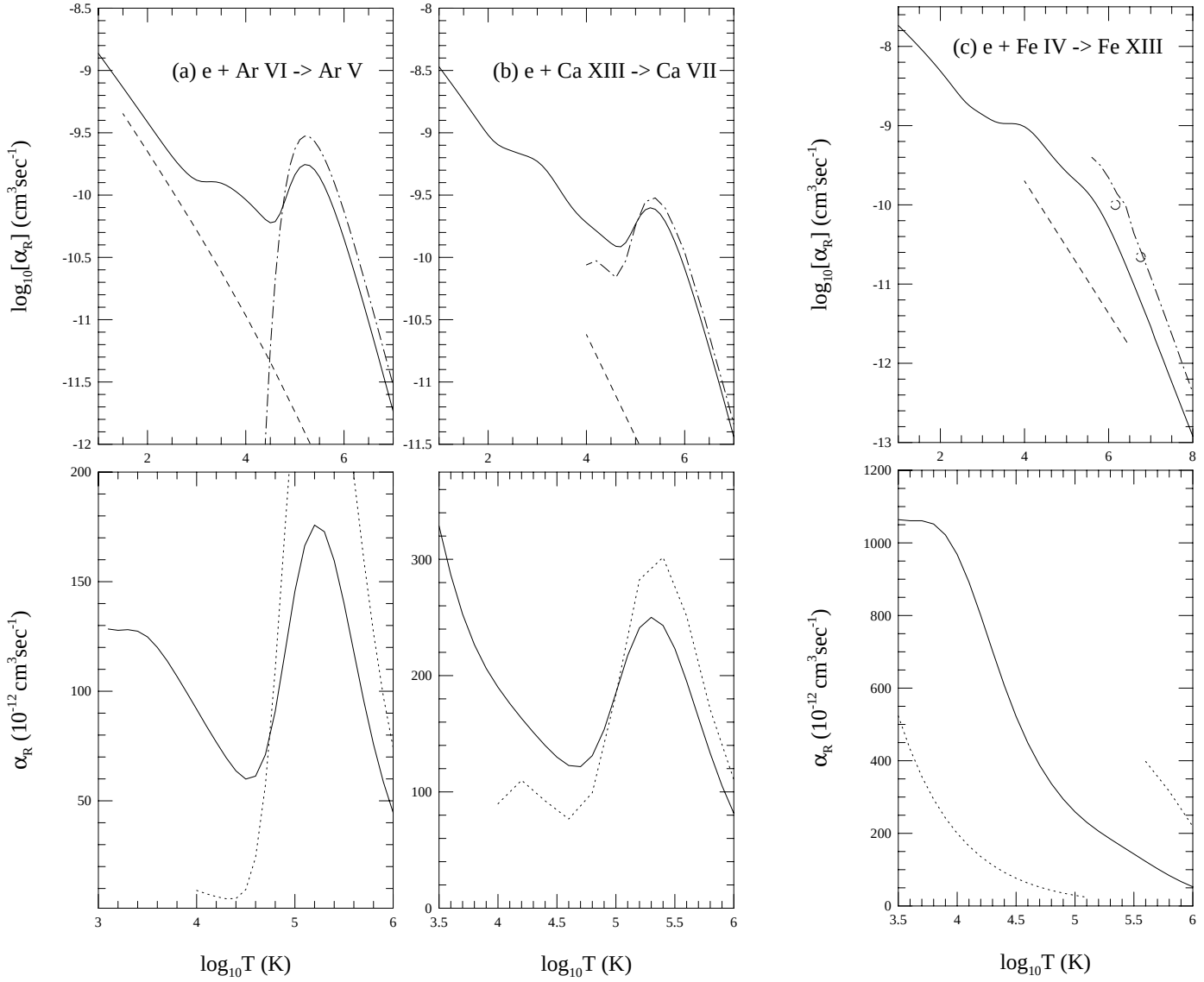

FIG. 5.—Total recombination rate coefficients $\alpha_R(T)$ of (*a*) e + Ar VI → Ar V, (*b*) e + Ca VIII → Ca VII, and (*c*) e + Fe XIV → Fe XIII. The top panels show α_R for a wide range of temperatures, while the bottom panels show the expanded features in the region where the rates go through the minimum. The solid curves are the present total rates in both panels, the dashed curves are the RR rates (Aldrovandi & Pequignot 1974 for Ar V, Shull & van Steenberg 1982 for Ca VII, and Woods et al. 1981 for Fe XIII), the dot-dashed curves (Shull & van Steenberg 1982 for Ar V, Jacobs et al. 1980 for Ca VII, and Woods et al. 1981 for Fe XIII) and the open circles for Fe XIII (Hahn 1989) are the high-temperature DR rates. The dotted curve in the bottom panels are the summed rates of RR and DR from previous calculations.

TABLE 4

TOTAL RECOMBINATION RATE COEFFICIENTS FOR Si-LIKE IONS[a]

	$\alpha_R(T)$				
$\log_{10} T$	Si I	S III	Ar V	Ca VII	Fe XII
1.0.....	5.02E−11	8.37E−10	1.37E−09	3.39E−09	1.84E−08
1.1.....	4.41E−11	7.40E−10	1.21E−09	3.00E−09	1.63E−08
1.2.....	3.87E−11	6.54E−10	1.07E−09	2.65E−09	1.44E−08
1.3.....	3.40E−11	5.77E−10	9.40E−10	2.34E−09	1.27E−08
1.4.....	2.99E−11	5.09E−10	8.29E−10	2.06E−09	1.12E−08
1.5.....	2.62E−11	4.49E−10	7.31E−10	1.81E−09	9.81E−09
1.6.....	2.30E−11	3.95E−10	6.43E−10	1.60E−09	8.59E−09
1.7.....	2.02E−11	3.48E−10	5.66E−10	1.40E−09	7.50E−09
1.8.....	1.77E−11	3.05E−10	4.97E−10	1.23E−09	6.53E−09
1.9.....	1.55E−11	2.68E−10	4.38E−10	1.08E−09	5.67E−09
2.0.....	1.36E−11	2.34E−10	3.85E−10	9.60E−10	4.89E−09
2.1.....	1.19E−11	2.04E−10	3.38E−10	8.66E−10	4.21E−09
2.2.....	1.05E−11	1.77E−10	2.97E−10	8.02E−10	3.60E−09
2.3.....	9.19E−12	1.54E−10	2.62E−10	7.62E−10	3.07E−09
2.4.....	8.06E−12	1.33E−10	2.31E−10	7.35E−10	2.63E−09
2.5.....	7.07E−12	1.14E−10	2.05E−10	7.11E−10	2.26E−09
2.6.....	6.20E−12	9.79E−11	1.83E−10	6.88E−10	1.97E−09
2.7.....	5.45E−12	8.37E−11	1.65E−10	6.68E−10	1.77E−09
2.8.....	4.79E−12	7.15E−11	1.50E−10	6.47E−10	1.61E−09
2.9.....	4.21E−12	6.10E−11	1.39E−10	6.23E−10	1.49E−09
3.0.....	3.72E−12	5.23E−11	1.32E−10	5.90E−10	1.38E−09
3.1.....	3.30E−12	4.51E−11	1.28E−10	5.45E−10	1.28E−09
3.2.....	2.94E−12	3.92E−11	1.28E−10	4.91E−10	1.19E−09
3.3.....	2.65E−12	3.43E−11	1.28E−10	4.34E−10	1.12E−09
3.4.....	2.40E−12	3.04E−11	1.27E−10	3.79E−10	1.08E−09
3.5.....	2.19E−12	2.73E−11	1.25E−10	3.29E−10	1.06E−09
3.6.....	2.01E−12	2.47E−11	1.20E−10	2.87E−10	1.06E−09
3.7.....	1.87E−12	2.26E−11	1.14E−10	2.53E−10	1.06E−09
3.8.....	1.76E−12	2.09E−11	1.07E−10	2.27E−10	1.05E−09
3.9.....	1.67E−12	1.94E−11	9.94E−11	2.06E−10	1.02E−09
4.0.....	1.60E−12	1.81E−11	9.18E−11	1.90E−10	9.68E−10
4.1.....	1.62E−12	1.69E−11	8.42E−11	1.76E−10	8.92E−10
4.2.....	1.83E−12	1.59E−11	7.68E−11	1.63E−10	8.00E−10
4.3.....	2.44E−12	1.54E−11	6.97E−11	1.51E−10	7.02E−10
4.4.....	3.54E−12	1.68E−11	6.37E−11	1.40E−10	6.07E−10
4.5.....	5.06E−12	2.23E−11	5.99E−11	1.30E−10	5.22E−10
4.6.....	6.67E−12	3.42E−11	6.13E−11	1.23E−10	4.49E−10
4.7.....	7.98E−12	5.28E−11	7.11E−11	1.22E−10	3.87E−10
4.8.....	8.66E−12	7.48E−11	9.08E−11	1.31E−10	3.37E−10
4.9.....	8.72E−12	9.51E−11	1.18E−10	1.53E−10	2.94E−10
5.0.....	8.24E−12	1.09E−10	1.46E−10	1.85E−10	2.59E−10
5.1.....	7.33E−12	1.14E−10	1.66E−10	2.17E−10	2.30E−10
5.2.....	6.28E−12	1.10E−10	1.76E−10	2.41E−10	2.06E−10
5.3.....	5.18E−12	1.00E−10	1.73E−10	2.50E−10	1.84E−10
5.4.....	4.16E−12	8.66E−11	1.60E−10	2.43E−10	1.64E−10
5.5.....	3.29E−12	7.20E−11	1.40E−10	2.23E−10	1.43E−10
5.6.....	2.54E−12	5.79E−11	1.18E−10	1.95E−10	1.23E−10
5.7.....	1.95E−12	4.54E−11	9.58E−11	1.64E−10	1.03E−10
5.8.....	1.48E−12	3.48E−11	7.58E−11	1.33E−10	8.39E−11
5.9.....	1.12E−12	2.63E−11	5.87E−11	1.05E−10	6.72E−11
6.0.....	8.44E−13	1.96E−11	4.46E−11	8.16E−11	5.28E−11
6.1.....	5.73E−13	1.45E−11	3.34E−11	6.21E−11	4.09E−11
6.2.....	4.24E−13	1.06E−11	2.48E−11	4.66E−11	3.12E−11
6.3.....	3.13E−13	7.71E−12	1.82E−11	3.46E−11	2.36E−11
6.4.....	2.26E−13	5.57E−12	1.33E−11	2.55E−11	1.77E−11
6.5.....	1.66E−13	4.02E−12	9.64E−12	1.86E−11	1.32E−11
6.6.....	1.22E−13	2.88E−12	6.96E−12	1.35E−11	9.80E−12
6.7.....	8.95E−14	2.06E−12	5.02E−12	9.80E−12	7.23E−12
6.8.....	6.57E−14	1.47E−12	3.59E−12	7.08E−12	5.34E−12
6.9.....	4.83E−14	1.05E−12	2.57E−12	5.04E−12	3.94E−12
7.0.....	3.55E−14	7.50E−13	1.84E−12	3.62E−12	2.90E−12
7.1.....	2.62E−14	5.34E−13	1.31E−12	2.59E−12	2.04E−12
7.2.....	1.94E−14	3.80E−13	9.35E−13	1.85E−12	1.50E−12
7.3.....	1.44E−14	2.70E−13	6.67E−13	1.32E−12	1.09E−12
7.4.....	1.07E−14	1.92E−13	4.75E−13	9.46E−13	7.93E−13
7.5.....	8.01E−15	1.36E−13	3.38E−13	6.76E−13	5.79E−13
7.6.....	6.03E−15	9.69E−14	2.41E−13	4.82E−13	4.23E−13
7.7.....	4.57E−15	6.89E−14	1.72E−13	3.44E−13	3.08E−13
7.8.....	3.49E−15	4.89E−14	1.22E−13	2.46E−13	2.25E−13
7.9.....	2.69E−15	3.48E−14	8.70E−14	1.75E−13	1.65E−13
8.0.....	2.09E−15	2.47E−14	6.19E−14	1.25E−13	1.20E−13

[a] Total Recombination Rate Coefficients, $\alpha_R(T)$ (in units of $cm^3\ s^{-1}$), for Si-like ions, Si I, S III, Ar V, Ca VII, and Fe XIII, in temperature range of $1.0 \leq \log_{10} T \leq 8.0$.

The earlier results were obtained mostly using simpler approximations. The RR rates were obtained from photoionization cross sections calculated in the central field approximation and in the hydrogenic approximation or through interpolation along isoelectronic sequences. The RR rates by Aldrovandi & Pequignot (1974) for Ar V (*dashed curve*) are considerably lower at low temperatures. These calculations did not include any autoionizing resonances. However, at very low temperatures, RR is expected to dominate since the electron energy is not usually high enough for exciting the autoionizing resonances. The RR rates by Aldrovandi & Pequignot curve slightly instead of rising sharply toward lower temperature. The high-temperature DR rates for Ar V by Shull & van Steenberg (1982) (*dot-dashed curve*), obtained through interpolation along isoelectronic sequence, overestimate the recombination rates. For Ca VII, Shull & van Steenberg (1982) interpolated the RR rates for a comparatively smaller temperature range (*dashed curve*), where they are considerably lower than the present rates. However, the DR rates for Ca VII by Jacobs et al. (1980) (*dot-dashed curve*) show a much better agreement, with the present rates differing by about 20% at the peak. Jacobs et al. calculated the rates in the isolated resonance approximation by including the autoionization to excited states of the recombining ion and by stabilizing the radiative transitions of the recombining electron, which reduces the DR contributions. The RR rates for Fe XIII obtained by Woods, Shull, & Sarazin (1981) in the intermediate-temperature range (*dashed curve*) underestimate considerably the total rates compared with the present ones. The dot-dashed curve for Fe XIII at high temperatures is the sum of α_{RR} and α_{DR} by Jacobs et al. (1977). Although they considered autoionization into the excited states, their rates appear to overestimate the total rate coefficient. The coupling of channels, which has lowered the DR rates more in the present calculations, is treated more precisely in the CC approximation than in the isolated resonance approximation. The two open circles are the DR rates of Fe XIII obtained by Hahn (1989) using the semi-empirical Burgess formula, and they are somewhat lower than those obtained by Jacobs et al. (1977) and higher than the present values.

The very high energy recombination rates, beyond the highest target threshold considered in the CC wave function expansion, have been obtained through the extrapolation of the photoionization cross section (Nahar & Pradhan 1994). Hence, the recombination rates are expected to be more uncertain at electron energies beyond the highest target threshold, i.e., at temperatures beyond 1.2×10^5 K for Si I, 3.5×10^5 K for S III, 5.7×10^5 K for Ar V, 7.9×10^5 K for Ca VII, and 1.1×10^6 K for Fe XIII.

Present results are estimated to be accurate to within 10%–30%. Relativistic effects are expected not to be very important for these ions; nonetheless, their inclusion could lead to improved accuracy. Present calculations have been computationally extensive, especially for Fe XIII. However, relativistic calculations would require perhaps an order of magnitude more of computing resources. Radiation damping of low-n autoionizing resonances is not included. The radiative rates for the dipole-allowed transitions for these ions (A_{fi} in Table 2) are several orders of magnitude lower than typical autoionization rates of 10^{13}–10^{14} s^{-1}. Hence, radiation damping should not have a significant effect on low-n resonances (a detailed discussion is given in Zhang, Nahar, & Pradhan 1999).

4. CONCLUSION

Total and partial photoionization cross sections of a large number of bound states, and total and state-specific recombination rate coefficients, are presented for the Si-like ions, Si I, S III, Ar V, Ca VII, and Fe XIII. Present data for photoionization cross sections are more complete than any previous calculations. The background photoionization cross sections of the ground states are generally featureless and are in good agreement with the earlier data. However, the excited state cross sections contain more resonance features because of larger target state expansions. More importantly, the calculated recombination rates are self-consistent with the photoionization cross sections.

The total electron-ion recombination rates exhibit a general pattern (e.g., Nahar & Pradhan 1994). Starting with a high recombination rate at low temperature, dominated by radiative recombination of low-energy electrons into very high-n states, the $\alpha_R(T)$ decreases but may exhibit low-temperature bump(s) due to recombinations via near-threshold autoionizing resonances. The $\alpha_R(T)$ reaches a minimum before being enhanced by high-temperature DR with high-energy electrons and falls off toward still higher temperatures because of the Maxwellian damping factor. Present total recombination rate coefficients show substantial differences with existing data for most cases.

The overall uncertainty in the electron-ion recombination data is estimated to be within 10%–30%, as is typical for CC $\boldsymbol{R}$-matrix calculations and as inferred from a comparison of calculated energies with the observed ones. Inclusion of relativistic effects would improve the accuracy, but the calculations are likely to be computationally prohibitive in the near future.[1]

This work has been partially supported by the US National Science Foundation and NASA. The computational work was carried out on the Cray T-94 at the Ohio Supercomputer Center.

[1] All photoionization and recombination data are available electronically from the author at nahar@astronomy.ohio-state.edu.

REFERENCES

Aldrovandi, S. M. V., & Pequignot, D. 1974, Rev. Brasileira Fis., 4, 491
Bell, R. H., & Seaton, M. J. 1985, J. Phys. B, 18, 1589
Berrington, K. A., Burke, P. G., Butler, K., Seaton, M. J., Storey, P. J., Taylor, K. T., & Yan, Yu. 1987, J. Phys. B, 20, 6379
Burgess, A. 1965, ApJ, 141, 1588
Cunto, W., Mendoza, C., Ochsenbein, F., & Zeippen, C. J. 1993, A&A, 275, L5
Eissner, W., Jones, M., & Nussbaumer, H. 1974, Comput. Phys. Commun., 8, 270
Hahn, Y. 1989, J. Quant. Spectrosc. Radiat. Transfer, 41, 315
Hummer, D. G., Berrington, K. A., Eissner, W., Pradhan, A. K., Saraph, H. E., & Tully, J. A. 1993, A&A, 279, 298
Jacobs, V. L., Davis, J., Kepple, P. C., & Blaha, M. 1977, ApJ, 211, 605
Jacobs, V. L., Davis, J., Rogerson, J. E., Blaha, M., Cain, J., & Davis, M. 1980, ApJ, 239, 1119
Nahar, S. N. 1995, ApJS, 101, 423
———. 1996a, ApJS, 106, 213
———. 1996b, Phys. Rev. A, 53, 2417

Nahar, S. N. 1999a, ApJS, 120, 131
———. 1999b, At. Data Nucl. Data Tables, 72, 129
Nahar, S. N., & Pradhan, A. K. 1991, Phys. Rev. A, 44, 2935
———. 1993, J. Phys. B, 26, 1109
———. 1994, Phys. Rev. A, 49, 1816
———. 1995, ApJ, 447, 966
———. 1997, ApJS, 111, 339
Nussbaumer, H., & Storey, P. J. 1983, A&A, 126, 75
Seaton, M. J. 1987, J. Phys. B, 20, 6363
Shull, J. M., & van Steenberg, M. 1982, ApJS, 48, 95
The Opacity Project Team. 1995–1996, The Opacity Project, Vols. 1 and 2 (Bristol: IOP)
Woods, D. T., Shull, J. M., & Sarazin, C. L. 1981, ApJ, 249, 399
Yu, Y., & Seaton, M. J. 1987, J. Phys. B, 20, 6409
Zhang, H. L., Nahar, S. N., & Pradhan, A. K. 1999, J. Phys. B, 32, 1459